Genetic Basis of De Novo Appearance of Carotenoid Ornamentation in Bare Parts of Canaries

Małgorzata Anna Gazda (ORCID) ,*,†,1,2 Matthew B. Toomey,*,†,3 Pedro M. Araújo,1,4 Ricardo J. Lopes,1 Sandra Afonso,1 Connie A. Myers,5 Kyla Serres,5 Philip D. Kiser,6 Geoffrey E. Hill,7 Joseph C. Corbo,5 and Miguel Carneiro*,1,2

1CIBIO/InBIO, Centro de Investigação em Biodiversidade e Recursos Genéticos, Universidade do Porto, Vairão, Portugal
2Departamento de Biologia, Faculdade de Ciências, Universidade do Porto, Porto, Portugal
3Department of Biological Science, University of Tulsa, Tulsa, OK
4MARE – Marine and Environmental Sciences Centre, Department of Life Sciences, University of Coimbra, Coimbra, Portugal
5Department of Pathology and Immunology, Washington University School of Medicine, St. Louis, MO
6Department of Physiology & Biophysics, School of Medicine, Gillespie Neuroscience Research Facility, University of California, Irvine, Irvine, CA
7Department of Biological Sciences, Auburn University, Auburn, AL
†These authors contributed equally to this work.
*Corresponding authors: E-mails: m.gazda@cibio.up.pt; mbtoomey@gmail.com; miguel.carneiro@cibio.up.pt.
Associate editor: Patricia Wittkopp

Abstract

Unlike wild and domestic canaries (*Serinus canaria*), or any of the three dozen species of finches in genus *Serinus*, the domestic urucum breed of canaries exhibits bright red bills and legs. This novel trait offers a unique opportunity to understand the mechanisms of bare-part coloration in birds. To identify the mutation producing the colorful phenotype, we resequenced the genome of urucum canaries and performed a range of analyses to search for genotype-to-phenotype associations across the genome. We identified a nonsynonymous mutation in the gene *BCO2* (beta-carotene oxygenase 2, also known as *BCDO2*), an enzyme involved in the cleavage and breakdown of full-length carotenoids into short apocarotenoids. Protein structural models and in vitro functional assays indicate that the urucum mutation abrogates the carotenoid-cleavage activity of BCO2. Consistent with the predicted loss of carotenoid-cleavage activity, urucum canaries tended to have increased levels of full-length carotenoid pigments in bill tissue and reduced levels of carotenoid-cleavage products (apocarotenoids) in retinal tissue compared with other breeds of canaries. We hypothesize that carotenoid-based bare-part coloration might be readily gained, modified, or lost through simple switches in the enzymatic activity or regulation of *BCO2* and this gene may be an important mediator in the evolution of bare-part coloration among bird species.

Key words: avian coloration, genetic mapping, color vision, retina.

Introduction

The hue and pattern of bird coloration has been a central arena for testing theories of signaling, assessment, and speciation (Mayr 1963; Andersson 1994; Hill and McGraw 2006a). The pigmentary and structural bases of avian coloration are now well understood (Hill and McGraw 2006b). The key missing piece to the puzzle of how and why conspicuous coloration evolves in birds is a better understanding of the genetic and molecular mechanisms controlling the production of color (Hubbard et al. 2010; Toews et al. 2017). Recent breakthroughs have begun to reveal the genes that control carotenoid pigmentation, which mediates most of the conspicuous red, orange, and yellow coloration in birds. *CYP2J19*, a cytochrome p450 gene, is implicated in the conversion of yellow to red carotenoids and consequently for much of the red coloration in birds (Lopes et al. 2016; Mundy et al. 2016).

SCARB1 plays a key role in carotenoid uptake mediating the presence or absence of coloration (Toomey et al. 2017). Here, we add to a growing understanding of the genetic basis of coloration in birds by revealing the mechanism for the de novo appearance of bill and leg coloration in canaries.

Domesticated canaries are derived from the island canary (*Serinus canaria*), a small finch with dull yellow carotenoid-based feather coloration and no carotenoid coloration in their bill or legs (Koch et al. 2016). Several centuries of selective breeding produced domestic canary birds with a fantastic diversity of yellow and red feather coloration, but until very recently no breed of canary had been produced that deposited carotenoids in their bills or legs (Birkhead et al. 2004). Indeed, none of the three dozen species of finches in the genus *Serinus* have red or yellow leg or bill coloration (Clement et al. 1993). Several decades ago, a canary with a
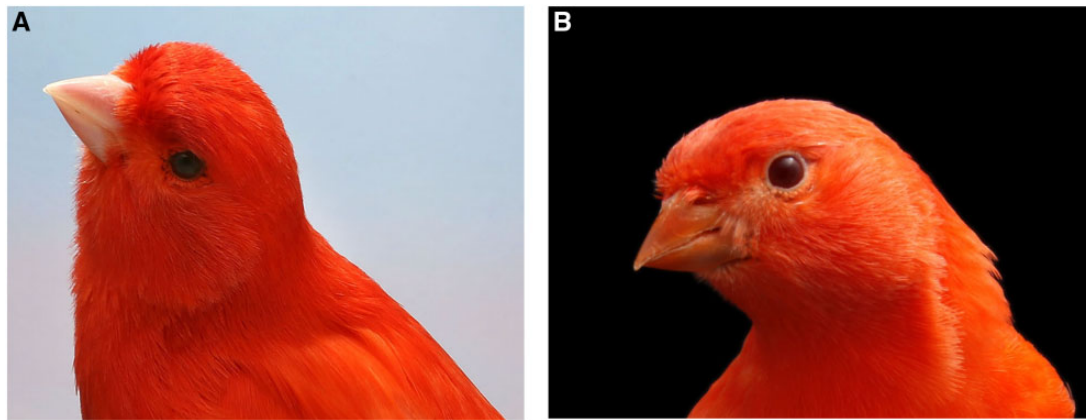
1

FIG. 1. Representative pictures of (A) lipochrome red canary (wild type) and (B) urucum canary (red form).

red bill and legs appeared spontaneously in a colony of red-factor canaries, a breed with bright red plumage coloration. Over subsequent years, this mutant canary founded a new breed of canary with bright red bills and legs, now called urucum canary (fig. 1). A yellow variant with pigmented beak and legs was subsequently derived and in this text we use the term urucum to refer to both red and yellow forms. The pigmentation in bare parts of urucum canaries follows an autosomal recessive pattern of inheritance. Thus, urucum canaries present a unique opportunity to identify a single genetic locus that enables birds to express a conspicuous new ornamental color trait.

To identify the causative mutation responsible for the expression of carotenoid-based pigmentation in bare parts in canaries, we resequenced the genome of urucum individuals and performed a range of analyses to search for genotype-to-phenotype associations across the genome. We identified a nonsynonymous point mutation in the gene BCO2, an enzyme that catalyzes the oxidative cleavage of both pro-vitamin A and non-pro-vitamin A carotenoids (Dela Seña et al. 2016) in birds and other vertebrates. We found a perfect association between presence/absence of the BCO2 mutation and bare-part coloration in canaries. Through protein structural models and in vitro functional assays, we confirm causality of the mutation and its effect on protein function.

Results

Carotenoid Content of Urucum Canary Tissues

The feathers and bare parts of the urucum canaries are brilliantly colored. To determine the pigmentary basis of the urucum phenotype, we used high-performance liquid chromatography (HPLC) to examine and compare carotenoid composition and accumulation in the beak and feather tissue of urucum and wild-type canaries with red and yellow plumage color backgrounds. We present qualitative descriptions of the comparisons between groups because robust statistical comparisons were not possible with the limited number of urucum samples ($n = 3$). Canaries carrying the urucum mutation tended to accumulate higher concentrations of

carotenoids in their beak tissues than wild-type birds (fig. 2A and supplementary figs. S1 and S2 and table S1, Supplementary Material online). The carotenoid concentration in the feathers of red canaries was significantly higher than in the feathers of yellow birds (Mann–Whitney $U = 0$, $n_1 = 5$, $n_2 = 4$, $P = 0.016$, fig. 2B and supplementary figs. S2 and S3 and table S2, Supplementary Material online), but feather carotenoid concentration did not appear to differ between urucum and wild-type birds (fig. 2B and supplementary table S2, Supplementary Material online).

A diverse suite of carotenoid pigments accumulate within the oil droplets of the cone photoreceptors of the avian retina where they modify spectral sensitivity and fine tune color discrimination (Goldsmith et al. 1984; Toomey et al. 2015; Toomey and Corbo 2017). To determine if and how the urucum mutation influences carotenoid accumulation in the retina, we used HPLC to examine and compare the retinal carotenoid profiles of urucum and wild-type canaries. The total accumulation of all carotenoid types in the retina did not appear to differ between urucum and wild-type birds (fig. 2C and supplementary figs. S4 and S5 and table S3, Supplementary Material online). However, when we examined specific components of the retinal carotenoid profile we found that apocarotenoids were very low or absent from the retinas of urucum canaries (fig. 2D). Apocarotenoids (e.g., galloxanthin and dihydrogalloxanthin) pigment the cone oil droplets of the blue (SWS2) cone photoreceptor and the principle member of the double cone and are hypothesized to be produced through the BCO2-mediated cleavage of dietary zeaxanthin (Toomey et al. 2016). This result suggests that urucum birds may have decreased carotenoid-cleavage activity. Both wild-type and urucum red-factor background canaries accumulated canthaxanthin in their retinas (supplementary fig. S6, Supplementary Material online), which is not typically a component of the avian retinal carotenoid profile (Goldsmith et al. 1984; Toomey et al. 2015; Toomey M, unpublished data). In some urucum individuals (fed normal diet with supplement as regular red birds), canthaxanthin constituted as much as 80% of the carotenoid content of the retina (supplementary table S3 and figs. S4–S6, Supplementary Material online).
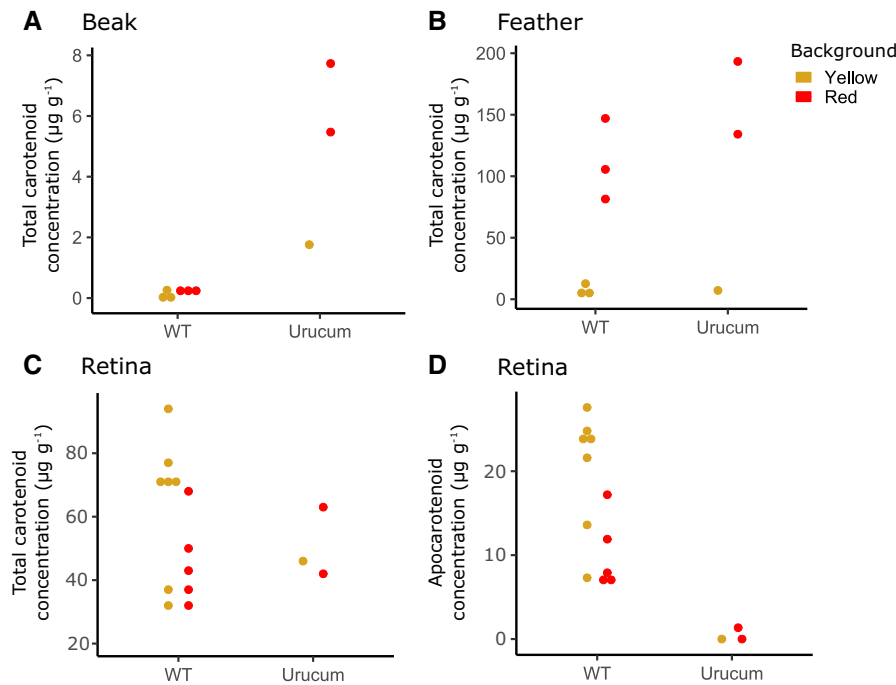
FIG. 2. Tissue carotenoid accumulation patterns among urucum and wild-type canaries. Points indicate the value for each individual sampled. The concentration of total carotenoids per gram of tissue are shown for (A) beak and (B) feathers of wild-type (WT) and urucum canaries with red-factor (denoted in red) or yellow lipochrome (denoted in yellow) genetic backgrounds. (C) The concentration of total carotenoids in the retina per gram of total protein sampled. (D) The concentration of carotenoid-cleavage products, apocarotenoids, in the retina per gram of total protein sampled. Details of the specific carotenoid composition of each tissue are available in supplementary tables S1–S3 and figures S1–S5, Supplementary Material online.

High-Resolution Mapping of the Urucum Phenotype

To investigate the genetic basis of bare-part coloration in urucum canaries, we performed whole-genome sequencing of a DNA pool of individuals of this breed ($n = 20$) to an effective coverage of $26\times$ (supplementary table S4, Supplementary Material online). Since the urucum breed was created through the fixation of a spontaneous mutation that emerged in red-factor canaries (Walker and Avon 1993), we compared urucum sequences with whole-genome resequencing data of a DNA pool of red lipochrome birds (wild type regarding bill coloration) ($n = 16$, coverage $= 17\times$) from a previous study (Lopes et al. 2016).

The urucum phenotype is transmitted in a manner consistent with a single recessive allele. Therefore, the genomes of both breeds are presumably very similar except in a single region controlling bare-part coloration. To search for regions of high differentiation between both breeds, we summarized allele frequency differentiation across the genome (scaffolds > 20 kb) using the fixation index (F_{ST}) and a sliding window approach (fig. 3A). We found that levels of genetic differentiation were low to moderate throughout most of the genome (mean $F_{ST} \sim 0.15$), but that one region displayed very high levels of F_{ST} when compared with the remainder of the genome. This region contained the top 36 values of the empirical distribution of F_{ST} (range $= 0.62–0.89$) and spanned a region of ~ 200 kb (715,000–930,000 bp) on scaffold NW_007931177, which is homologous to zebra finch chromosome 24 region around 1,362,685–1,644,140. Using a backcross mapping population (see Materials and Methods), we found a perfect association between our candidate region and bare-part coloration: All wild-type individuals ($n = 11$) were heterozygous for a single-nucleotide polymorphism (SNP) diagnostic between the urucum and wild-type parental individuals, and all birds exhibiting the urucum phenotype ($n = 7$) were homozygous for the allele present in the parental urucum individuals.

We next carried out identical-by-descent (IBD) mapping (fig. 3B) to increase the resolution at the candidate locus, under the assumption that the urucum mutation emerged a single time within a haplotype that should be shared by all urucum individuals. We genotyped 29 variants selected from the whole-genome resequencing data in a larger cohort of birds, including urucum individuals ($n = 24$) as well as individuals ($n = 14$) belonging to several breeds lacking coloration in bare parts. Unlike other breeds, we found that urucum canaries were homozygous for a large continuous genomic segment defined by 13 SNPs, spanning a physical interval of 104 kb (770,364–874,443) that harbored 8 protein-coding genes: NCAM1, PTS, BCO2, TEX12, IL18, SDHD, LOC103822986, and DLAT (fig. 3B and supplementary table S5, Supplementary Material online). Of these, BCO2 represents a strong candidate for the gene underlying the urucum phenotype since it encodes an enzyme that is known to cleave carotenoids (Kiefer et al. 2001; Amengual et al. 2011) and has been previously implicated in carotenoid pigmentation of the integument in birds and reptiles (Eriksson et al. 2008; Toews et al. 2016; Andrade et al. 2019; Fallahshahroudi et al. 2019).
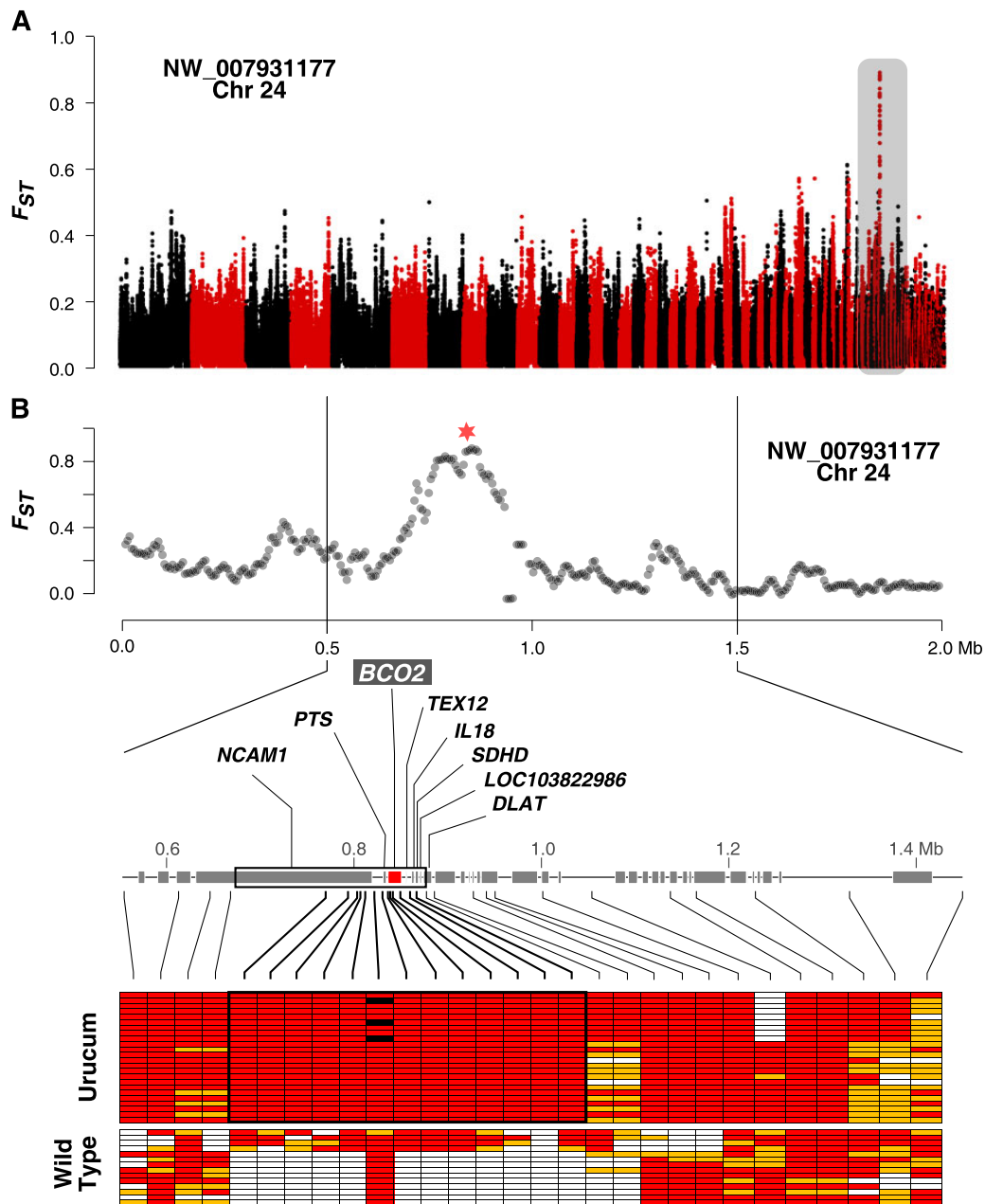
FIG. 3. Mapping of the urucum mutation. (*A*) Selective sweep mapping. F_{ST} between urucum and lipochrome red breed across the genome. Each dot represents F_{ST} in 20-kb windows iterated every 5 kb. The different scaffolds are presented along the *x* axis in the same order as they appear in the canary reference genome assembly. (*B*) F_{ST} zoom-in and IBD mapping. (Top) F_{ST} in 20-kb windows iterated every 5 kb across the outlier region (delineated by vertical lines). A red star marks the location of the nonsynonymous mutation. (Bottom) The protein-coding genes found within this region are indicated by gray boxes. For the IBD analysis, 29 SNPs were genotyped for 24 urucum canaries and 14 individuals belonging to 3 breeds with yellow, red, and white coloration. Alleles more common in urucum canaries are represented by red boxes, alternative alleles are represented in white, and heterozygous are represented in orange. The black-outlined box indicates a segment of high homozygosity in urucum canaries and black boxes indicate missing data.

An Amino Acid Substitution at a Universally Conserved Position in *BCO2* Is Perfectly Associated with the Urucum Phenotype

We next screened the IBD interval for potential causative mutations using the whole-genome resequencing data. First, we examined this region of the genome for structural rearrangements that could be associated with the phenotype (see Materials and Methods), but we did not detect any plausible candidate. Then, we assessed single point mutations and small indels that could alter protein structure (nonsynonymous, frameshift, stop, and splicing-site mutations). We searched for variants characterized by strong allele frequency differentiation between urucum and wild-type birds (delta allele frequency >0.8) and with high conservation scores (>0.9) derived from multispecies alignments obtained from a previous study (Toomey et al. 2017). One single point mutation met these criteria located at nucleotide position 837,806, which was predicted to be a nonsynonymous
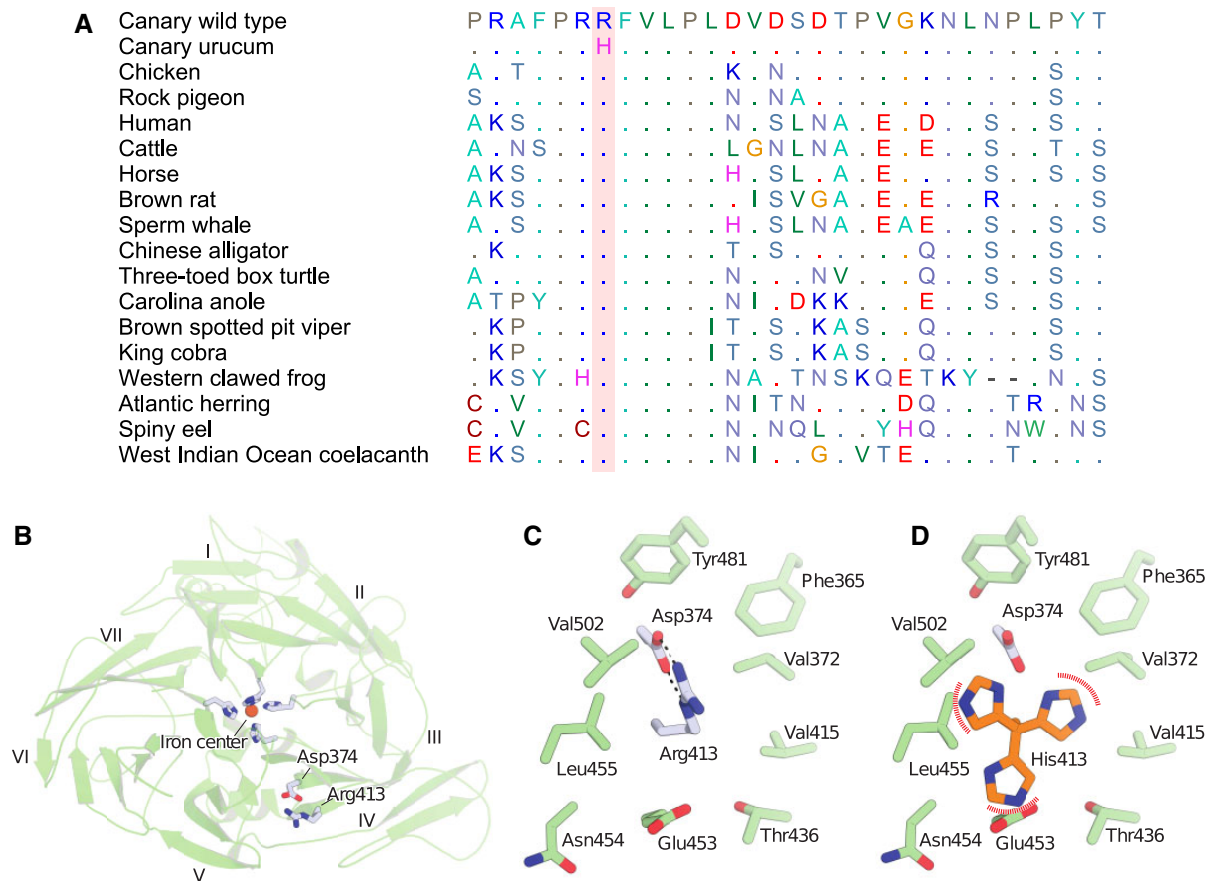
Fig. 4. Structural consequences of the R413H substitution in canary *BCO2*. (A) Multispecies alignment of vertebrates surrounding the candidate amino acid substitution in the highly conserved exon 9 of *BCO2* (the amino acid substitution is highlighted in pink). The dots represent the same nucleotide as the reference wild-type canary allele at a given position. (B) Homology model of canary *BCO2* based on an RPE65 template. Blades are numbered according to convention. (C) Close-up view of R413 forming a twin salt bridge interaction with Asp374 within a pocket composed of predominantly nonpolar side chains. (D) Substitution of Arg413 with His results in predicted steric clashes with surrounding side chains that would disrupt the protein structure or cause a protein-folding defect.

mutation in the exon 9 of the *BCO2* gene. This variant results in the substitution of a histidine for an arginine at residue 413 of the protein (R413H) that could potentially affect *BCO2* activity (see below). We genotyped the nonsynonymous variant in the cohort of urucum samples used for the IBD analysis above, and consistent with an autosomal recessive mode of inheritance, we found that all 24 individuals were homozygous for the allele encoding the amino acid histidine. Interestingly, domesticated canaries expressing yellow carotenoids in their bare parts (*n* = 4), which have emerged more recently, were also homozygous for the same nonsynonymous variant, suggesting the same genetic basis for barepart coloration in both red and yellow birds. A multispecies alignment of the *BCO2* protein, including 175 species from all major vertebrate groups revealed that this amino acid is universally conserved (fig. 4A and supplementary fig. S7, Supplementary Material online).

To help define the structural consequences of the R413H substitution in *BCO2*, we first generated a homology model of canary *BCO2* using the crystal structure of a BCO2 paralog, bovine RPE65, as a template (fig. 4B). The sequences share ~42% sequence identity suggesting that the *BCO2* model

should have an overall root mean square deviation from the true structure of ~1.2 Å (Chothia and Lesk 1986). Inspection of the model revealed that Arg413 is predicted to form a salt bridge interaction with Asp374 at the interface between beta sheets IV and V, a location distant from the enzyme iron center. The same type of electrostatic interaction is formed between equivalent residues of other members of the carotenoid-cleavage oxygenase family of enzymes, including *Synechocystis* ACO (Kloer et al. 2005) and bovine RPE65 (Kiser et al. 2009), indicating its structural or functional importance. Indeed, Arg-carboxylate salt bridges are known to contribute substantially to protein thermal stability (Singh et al. 1987). The Arg-Asp pair is located in a hydrophobic pocket formed between blades IV and V of the beta-propeller domain. The electrostatic complementarity of these residues appears important for maintaining an overall neutral charge within the apolar environment (fig. 4C). In silico substitution of His for Arg at position 413 resulted in severe steric clashes in all rotameric orientations of the His residue, which could not be resolved by secondary rotamer changes in the involved residues (fig. 4D). This observation suggests that the R413H could cause structural distortion of the protein,
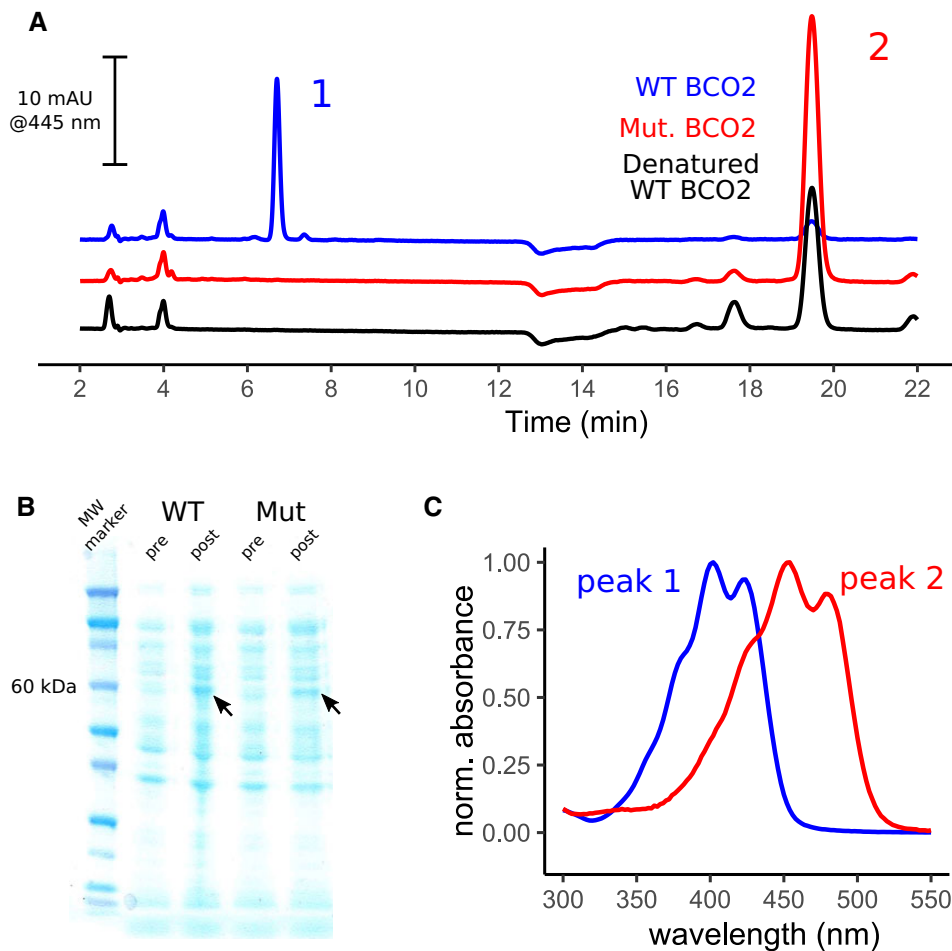
FIG. 5. In vitro assay of the cleavage activity of urucum and wild-type variants of BCO2. (A) Representative HPLC chromatograms of carotenoids extracted from reactions containing canthaxanthin substrates and wild-type, mutant, or wild-type heat-denatured bacterial lysates. (B) A Coomassie-stained SDS-PAGE gel visualizing protein expression in the BL21 DE3 cultures before (pre) and after (post) the induction of recombinant protein expression. Arrowheads indicate the enrichment of an ∼60-kDa band that is consistent with the induction of the expression of the recombinant wild-type (WT) and mutant (Mut) BCO2. (C) UV–Vis light absorbance spectra of peaks 1 and 2. Note that these samples have been reduced with sodium borohydride and the canthaxanthin substrate (peak 2) has been reduced to isozeaxanthin (β,β-carotene-4,4′-diol). The short retention time and short wavelength shifted absorbance spectrum of peak 1 is consistent with an apocarotenoid which we hypothesize to be 10′-Apo-β-carotene-4,10′-ol. We found no evidence of this apocarotenoid in the mutant or denatured BCO2 assays.

leading to a possible loss of activity. Alternatively, the substitution could cause a gross protein-folding defect via these steric clashes or through electrostatic destabilization. Overall, the striking conservation of the amino acid position, together with its predicted three-dimensional environment, strongly suggests that this mutation has severe functional consequences.

Although our evidence suggested a functional mutation in urucum BCO2, previous studies have linked carotenoid-based skin color to regulatory mutation at this locus (e.g., Eriksson et al. 2008). To evaluate whether regulatory mutations could also play a role in the urucum phenotype, we examined the allele-specific expression of BCO2 in the beak tissue of an individual heterozygous for the urucum and wild-type alleles. If cis-acting regulatory mutations are driving expression differences in BCO2, then one allele should be expressed preferentially. Using the nonsynonymous position as a marker for allelic identity, we found that the number of reads containing

the wild-type and urucum alleles of BCO2 was similar (48% vs. 52%, out of a total 193,155 reads overlapping the exon of this gene). We therefore conclude that the urucum phenotype is unlikely to be the result of cis-regulatory differences between the two alleles.

Functional Analysis Shows That the BCO2 Mutation Results in Compromised Enzymatic Activity

To determine if and how the candidate causal variant altered the carotenoid-cleavage activity of BCO2, we evaluated the ability of wild-type and urucum BCO2 to cleave zeaxanthin and canthaxanthin substrates. We found that bacterial lysates containing recombinantly expressed wild-type BCO2 readily cleaved both carotenoid substrates and generated apocarotenoid products (fig. 5 and supplementary fig. S8, Supplementary Material online). In contrast, lysates containing the urucum BCO2 variant, with the R413H substitution, did not produce any detectable apocarotenoids from a

canthaxanthin substrate (fig. 5 and supplementary fig. S8, Supplementary Material online). The reactions containing the mutant BCO2 variant retained substantially more substrate than the wild-type reaction (fig. 5). With the zeaxanthin substrate, we observed small amounts of apocarotenoid in the urucum BCO2 assay (supplementary fig. S8, Supplementary Material online). However, these trace amounts were also present in our negative control (heat-denatured lysate), therefore, we believe that these trace amounts of apocarotenoid may be a product of nonenzymatic oxidation (Yanishlieva et al. 1998). Taken together, our analyses indicate that the urucum mutation compromises the enzymatic activity of BCO2.

Discussion

Through genomic and biochemical analyses of the urucum canary breed, we identified a single-nucleotide nonsynonymous mutation affecting an evolutionarily invariant amino acid that results in de novo carotenoid-based coloration of the bill and legs. This mutation in the BCO2 gene disables the enzyme's carotenoid-cleavage activity, thereby causing a marked increase in the concentrations of intact carotenoids in tissues. The increase in carotenoid pigmentation of beak, legs, and skin of the urucum breed suggests that degradation of carotenoids by BCO2 is a key mechanism for regulating the presence or absence carotenoid coloration in these tissues in birds and could be an important target of selection in the evolution of color patterns.

Previous studies have implicated BCO2 in species-typical carotenoid coloration. Many breeds of domestic chickens have yellow legs but the wild progenitor of chickens, the red junglefowl (Gallus gallus), has gray legs lacking carotenoid coloration. Using QTL analysis, Eriksson et al. (2008) mapped the yellow leg coloration phenotype to a genomic region that contains BCO2. The authors found a tissue-specific reduction in BCO2 in the legs of yellow birds, suggesting a cis-regulatory mutation affecting BCO2 expression, but the causal mutation was not identified. The authors suggested that this mutation had been acquired through introgression from a sister species, the gray junglefowl (Gallus sonneratii), which has yellow legs. Subsequently, BCO2 has been implicated in carotenoid coloration in various animal groups, such as warblers (Toews et al. 2016) and lizards (Andrade et al. 2019), as well as in control of fat and milk color in domestic animals (Tian et al. 2010; Våge and Boman 2010; Strychalski et al. 2015). Here, we show that a single nonsynonymous mutation in BCO2 can lead to large changes in the ornamental color pattern of a songbird. The carotenoid-cleaving activity of BCO2 presents a mechanism by which carotenoid-based bare-part coloration might be readily gained, modified, or lost through simple regulatory switches controlling tissue-specific expression of BCO2 or changes in its enzymatic activity. This relatively simple mechanism is consistent with the apparent evolutionarily rapid loss and gain of bare-part coloration in many groups of birds (Iverson and Karubian 2017) and raises the possibility that these colorful traits might be particularly labile through the course of evolution.

In addition to bare-part pigmentation, the retinal carotenoid profiles of urucum canaries differ from wild-type birds, indicating that BCO2 plays an important role in the pigmentation of the oil droplets that fine tune the spectral sensitivity of avian cone photoreceptors. In the urucum canaries, we observed little or no apocarotenoid pigment in the retina. Apocarotenoid pigments selectively accumulate in the oil droplets of the blue cone (SWS2) photoreceptor and the principal member of the double cone photoreceptor (Toomey et al. 2015, 2016). We previously speculated that the selective accumulation of apocarotenoids is mediated by the cone subtype-specific expression of the BCO2 within the blue and double cones (Toomey et al. 2016). The reduction or absence of apocarotenoid pigmentation in the retinas of urucum canaries supports this hypothesis.

Detailed understanding of carotenoid metabolism and its biochemical and physiological importance hold the potential for better understanding of not only ornamental coloration in birds but also the role of micronutrients in health and disease in vertebrates more generally. The pathophysiology of the urucum mutation has not been fully characterized, but breeders have reported that urucum birds suffer from problems with balance, motor abilities, coordination, inactivity, and vision. Although we have not directly investigated these problems, the disruption of BCO2 function is likely to result carotenoid overaccumulation in critical organ systems like the liver and brain. Previous studies have shown that high levels of carotenoid accumulation can have negative physiological effects. For example, in American goldfinches (Carduelis tristis), long-term exposure of tissues to high levels of carotenoids resulted in a gradual deterioration of skeletal muscle tissue and consequent defects in flight performance (Huggins et al. 2010). In mouse, BCO2 knock out results in the accumulation of abnormally high levels of xanthophyll carotenoids in the liver and other tissues (Amengual et al. 2011). BCO2 mutant mice show evidence of mitochondrial dysfunction, elevated oxidative stress, and liver steatosis, indicating that BCO2 plays an important role in maintaining carotenoid homeostasis and protecting against the potentially damaging effects of these pigments (Amengual et al. 2011). Similar detrimental effects of BCO2 knockdown have also been demonstrated in developing zebra fish (Danio rerio) and human cell lines, indicating that the role of BCO2 in carotenoid homeostasis is broadly conserved (Lobo, Amengual, et al. 2012; Lobo, Isken, et al. 2012). Our observations suggest that the interplay of the signaling benefits of carotenoid coloration and potential physiological costs of concentrations of these pigments in tissues may be mediated by regulation of BCO2.

Materials and Methods

HPLC Analyses in Feathers, Beak, and Retina

We used HPLC to determine the composition and concentrations of carotenoid pigments in the tissues of two urucum canaries with a red-factor background, one urucum canary with a yellow plumage background, three to five red-factor canaries that were wild type for the urucum mutation and three to seven yellow lipochrome canaries that were wild type

for the urucum mutation. To assay the carotenoid content of the feathers, we plucked ten feathers from the nape of each bird and measured the total mass of the feathers sampled from each individual on a laboratory balance. We extracted pigments by incubating the feather for 6 h at 65 °C in 2 ml of acidified pyridine (McGraw et al. 2005). We then added 2 ml of distilled water and extracted with 2 ml of hexane:*tert*-methyl butyl ether (1:1 vol:vol). We collected the hexane:-*tert*-methyl butyl ether fraction, evaporated to dryness under a stream of nitrogen, and resuspended in 200 µl of methanol:acetonitrile 1:1 (vol:vol). We injected 50 µl of each extract into an Agilent 1100 series HPLC with an YMC carotenoid 5.0-µm column (4.6 mm × 250 mm, YMC). We separated pigments with a gradient mobile phase consisting of acetonitrile:methanol:dichloromethane (44:44:12) (vol:vol:vol) for 0–11 min then a ramp up to acetonitrile:methanol: dichloromethane (35:35:30) from 11 to 21 min followed by a return to isocratic conditions through 35 min. The mobile phase was pumped at a constant rate of 1.2 ml/min and the column maintained at 30°C for the entirety of the run. We monitored the samples with a photodiode array detector at 400, 445, and 480 nm and identified and quantified carotenoids as described in Toomey et al. (2017).

We measured the retinal carotenoid content following previously published methods (Toomey et al. 2017). Briefly, we homogenized the retinas in phosphate buffered saline and extracted with hexane:*tert*-methyl butyl ether (1:1 vol:vol). We divided each sample in two and saponified with weak (0.02 M NaOH in methanol) or strong (0.2 M NaOH) base to optimize the recovery of ketocarotenoids or other carotenoid classes, respectively. We separated and quantified carotenoids on the HPLC system described above. Chromatographic conditions identical to feather analyses were used for the keto-carotenoid portion of the sample. The strong base samples were run under modified conditions to optimize the separation of apocarotenoids. For these samples, we cooled the column to 18°C and pumped mobile phase at a constant rate of 1.0 ml/min. We used a gradient mobile phase beginning with acetonitrile:methanol (50:50) for 9 min, followed by a ramp up to acetonitrile:methanol:dichloromethane (44:44:12) (vol:vol:vol) from 9 to 11 min, isocratic through 21 min, then a second ramp up to acetonitrile:methanol:dichloromethane (35:35:30) from 21 to 26 min followed by isocratic conditions through 35 min.

The extractions of carotenoids from the beak tissue proved challenging and we used two different methods depending on the color background of the individual. For all individuals, we cut a ~0.5-cm^2 portion of the lower mandible and measured total wet mass on a laboratory balance. For the individuals with a yellow plumage background, we extracted carotenoids with acidified pyridine as described above for the feather analyses. We attempted pyridine extraction for the individuals with the red plumage background but found that the yield of carotenoids was poor and the tissue retained its color. As an alternative, we ground the beak tissue for 30 min at 4,000 rpm with a bead mill (BeadBug, Benchmark Sci., Edison, NJ) using 10–2-mm zirconia beads in 1 ml of methanol. We centrifuged the resulting homogenate,

collected the methanol supernatant, and dried under a stream of nitrogen. We repeated this extraction three times for each sample and pooled the resulting supernatants for each sample. The carotenoid pigments recovered with the methanol extraction were esterified. Therefore, we saponified the samples with weak (red background) or strong (yellow background) base as described for the retina samples. We separated, identified, and quantified carotenoids with HPLC as described for the feather samples. The methanol extraction yielded a mean of 7.3× more carotenoid than the pyridine extraction of the red background samples. In contrast, the methanol extraction of the yellow background samples yielded only 33% of the carotenoid recovered with the pyridine extraction. Therefore, we report the results for the pyridine extraction for yellow background individuals and methanol extraction for the red background individuals.

Whole-Genome Resequencing, Read Mapping, and SNP Calling

To study the genetic basis of bare-part coloration in canaries, we performed whole-genome resequencing of a DNA pool of urucum individuals ($n = 20$). Briefly, blood was collected into a heparin-free capillary tube and immediately transferred into a vial with 96% ethanol. For DNA sequencing, we extracted genomic DNA from blood using an EasySpin Genomic DNA Kit SP-DT- 250 (Citomed), followed by a RNAse A digestion step. DNA quality and purity assessment were performed through spectrophotometry (Nanodrop) and fluorometric quantitation (Qubit dsDNA BR Assay Kit, ThermoScientific). Paired-end sequencing libraries for Illumina sequencing were then generated using the TruSeq DNA PCR-free Library Preparation Kit (Illumina, San Diego, CA) according to the manufacturer protocol and sequenced using 150-bp paired-end reads on an Illumina instrument (supplementary table S4, Supplementary Material online). Whole-genome sequencing data have been deposited in GenBank under the bioproject PRJNA559291.

The reads were trimmed with the program *Trimmomatic* (v. 0.36) (Bolger et al. 2014) using the following parameter settings: TRAILING = 15, SLIDINGWINDOW = 4:20, and MINLEN = 30. Sequencing reads were then mapped to the canary reference genome assembly (SCA1; GenBank assembly accession: GCA_000534875.1) (Frankl-Vilches et al. 2015) with *BWA-MEM* (Li and Durbin 2010), followed by local realignment performed using *GATK RealignerTargetCreator* and *IndelRealigner* options (McKenna et al. 2010). SNP calling was performed using the Bayesian haplotype-based method implemented in *Freebayes* (v0.9.21-26-gbfd9832) (Garrison and Marth 2012).

Genome-Wide Analysis of Genetic Differentiation

To identify the genomic region containing the urucum factor, we summarized genetic differentiation between urucum and red lipochrome canaries (data from a previous study [Lopes et al. 2016]) in windows of 20 kb moved in steps of 5 kb across the genome using the fixation index (F_{ST}). F_{ST} estimates for each window were obtained by means of an unbiased estimator that corrects for unequal sample sizes across positions

due to differences in the depth of coverage, as implemented in the *PoPoolation2* package (Kofler et al. 2011). We utilized the following filters: 1) a per base Phred quality score of 20 or higher, 2) a minimum coverage of 10× per position, 3) a maximum coverage of three times the average coverage per pool, and 4) at least four reads supporting the minor allele in polymorphic sites. Only windows that passed our quality filters in ≥30% of positions were kept.

Crosses and Linkage Analysis

For linkage analysis, we established crosses between urucum individuals and red lipochrome canaries. The resulting F1 individuals (six pairs) were backcrossed to urucum canaries. From these backcrosses, we obtained 18 individuals and 7 expressed red coloration in their beaks and bare parts (expected to be homozygous for the urucum factor), whereas 11 were wild type (expected to be heterozygous for the urucum factor). Blood was collected from all individuals and used for DNA extraction as described above. To test for linkage between the candidate genomic region (see Results) and the urucum phenotype in our pedigree, we genotyped an SNP by means of Sanger sequencing of a small amplicon (supplementary table S6, Supplementary Material online). Animal care complied with national and international regulations for the maintenance of live birds in captivity (Federation of European Laboratory Animal Science Associations).

Genotyping for IBD Mapping

We performed IBD mapping by genotyping a panel of 29 SNPs located in the vicinity of our candidate region both in urucum and wild-type individuals. The SNPs were randomly chosen from whole-genome resequencing data of several breeds and wild canaries obtained as part of a previous study (GenBank bioproject PRJNA300534 [Lopes et al. 2016]). Blood and DNA were extracted as described above. We genotyped 24 urucum individuals, which are supposed to be homozygous for the causative mutation, and 14 other color canaries belonging to 3 breeds (white dominant, $n = 4$; lipochrome yellow, $n = 5$; lipochrome red, $n = 5$). Genotyping was carried out using Sequenom (San Diego, CA) iPlex technology and detected on a Sequenom MassArray K2 platform available at the Instituto Gulbenkian de Ciência (Lisbon, Portugal). Sequenom MassARRAY Assay Design 3.0 software was used to design primers and establish the multiplex conditions. The resulting spectra and plots were manually inspected, and software genotype calls were corrected whenever required. Individual genotypes are available as a supplementary file S2, Supplementary Material online.

SNP/Indel Functional Annotation

We functionally annotated SNP and indel variants using the genetic variant annotation and effect prediction toolbox *SnpEff* (Cingolani et al. 2012). To search for causative mutations within our candidate region, we screened our candidate regions for variants that could potentially alter protein structure and function, such as nonsynonymous, frameshift, STOP, and splice site mutations.

Detection of Structural Rearrangements

The identification of structural variants within the candidate region was performed using three approaches: 1) *Breakdancer* (Chen et al. 2009), which uses read pair orientation and insert size, 2) *DELLY* (Rausch et al. 2012), which uses paired-end information and split-read alignments, and 3) *LUMPY* (Layer et al. 2014), which uses a combination of multiple signals including paired-end alignment, split-read alignment, and read-depth information. Candidate structural variants were manually inspected using *IGV* (Robinson et al. 2011) and intersected with the canary genome annotation (Frankl-Vilches et al. 2015).

Phylogenetic Conservation and Protein Structural Modeling

We extracted *BCO2* protein sequences from NCBI and checked for the conservation of the mutated amino acid in other species. We included 175 vertebrate species from a wide of taxonomic groups, including mammals, birds, amphibians, fish, and reptiles. Sequences were aligned using *ClustalW* multiple alignment implemented in *BioEdit* v7.0.5 (Hall 1999).

To infer the impact of the candidate nonsynonymous mutation in the protein structure of *BCO2*, we generated a homology model of canary BCO2 through the Swiss-Model server (Waterhouse et al. 2018) using bovine RPE65 as the template (PDB accession code: 4RYZ) (Zhang et al. 2015). The R417H substitution and rotamer analysis were performed using *Coot* (Emsley et al. 2010). Images of the wild-type and mutant structural models were generated using *Pymol* (Schrödinger, LLC).

Allelic Imbalance

We evaluated whether regulatory variation could explain the urucum phenotype by accessing allelic imbalance in the beak of a F1 individual from a cross between a urucum bird and wild-type individual (i.e., heterozygous for the urucum factor). Birds were euthanized following practices outlined by the American Veterinary Medical Association and approved by the ethical commission of CIBIO. We collected beak samples from the keratinized layer of the upper mandible epidermis. After dissection, the tissue was snap-frozen and stored at −80 °C until RNA extraction. RNA was extracted using the RNeasy Mini Kit (Qiagen), followed by cDNA synthesis using ∼1 µg of RNA and the GRS cDNA Kit (GRiSP). To quantify the relative expression of each allele (mutation or wild type), we designed primers to amplify a small fragment from cDNA overlapping the nonsynonymous mutation associated with the urucum phenotype (supplementary table S6, Supplementary Material online). Primers were located on exon–exon junctions to avoid spurious amplification from genomic DNA. Amplification of the cDNA template with 5′ labeled primers was done with the protocol described in Andrade et al. (2019). Amplicons were sequenced on an Illumina MiSeq system (MiSeq v3 500-cycle kit, 2x250 bp reads). To calculate the relative proportion of alleles expressed in the beak of the heterozygous individual, we mapped the reads with *BWA-MEM* (Li and Durbin 2010) on a reference containing just the *BCO2* cDNA sequence and counted the

number of reads corresponding to the reference and alternative alleles.

Functional Analysis of *BCO2* Wild-Type and Mutant Proteins

We assayed recombinantly expressed wild-type and mutant *BCO2* enzymes following methods adapted from Mein et al. (2011). We amplified the coding sequence of wild-type *BCO2* from the cDNA of a red-factor canary with the primers listed in supplementary table S6, Supplementary Material online, using Phusion Hot Start PCR master mix (M0536, NEB Inc, Ipswich, MA) following the manufacturer's suggested conditions. We cloned this amplicon into the pET28a vector at the *Ned*1 and *Xho*1 restriction sites and confirmed by Sanger sequencing (Eurofins, Louisville, KY). We then introduced the candidate variant into this construct with site-directed mutagenesis by PCR. The primers and procedure for mutagenesis are detailed in supplementary table S6, Supplementary Material online.

We transformed BL21 De3 cells with the wild-type and mutant constructs, grew 1 l liquid cultures of each, and induced protein expression at 16°C overnight (16 h) with Isopropyl β-D-1-thiogalactopyranoside following the suggested methods of the vector manufacturer (EMD Biosciences, Madison, WI). We confirmed the expression of the recombinant enzymes by visualizing protein expression in pre- and post-induction cultures on an SDS-PAGE gel. We pelleted bacterial cultures by centrifugation and resuspended pellets in Tricine buffer (50 mM Tricine, 100 mM NaCl, 1% Tween 40) and lysed cells with a cycle of freeze–thaw and brief sonication. We centrifuged the lysed cells at 10,000 × g for 30 min at 4°C, collected the supernatant, and measured total protein concentration of the lysates (Pierce BCA Protein Assay Kit, ThermoFisher, Waltham, MA). We then used these crude lysates to assayed enzyme activity as described below.

We prepared carotenoid substrates by fractioning all-trans-zeaxanthin and all-trans-canthaxanthin from commercial carotenoid additives (Optisharp, Carophyll Red, DSM Inc, Heerlen, the Netherlands) with HPLC. We evaporated the purified carotenoids to dryness under a stream of nitrogen and resuspended by sonication in 2.5 ml of Tricine buffer with 1.6% Tween 40. We combined 400 µl of each carotenoid suspension with a volume of each enzyme lysate containing 1 mg of total protein and supplemented the reaction with 10 µM FeSO4 and 0.3 mM dithiothreitol. We incubated these reactions in the dark at 37°C, shaking at 180 rpm, for 2 h. As a negative control, we denatured proteins by boiling the lysates at 100°C for 20 min and assayed as above. We extracted the reaction products by adding 1 ml of ethanol vortexing briefly, followed by 2 ml of hexane:*tert*-butyl methyl ether (1:1), centrifuging briefly and collecting the upper phase. We dried these extracts under a stream of nitrogen and then treated with sodium borohydride to reduce and stabilize apocarotenoid aldehyde products of *BCO2* cleavage. To do this, we resuspended the dried extracts in 1 ml of ethanol, added a few crystals of sodium borohydride, capped reaction tubes with nitrogen, and incubated for 30 min in the dark. We then added 2 ml of deionized water to the reaction and extracted

again with 2 ml of hexane:*tert*-butyl methyl ether. We again dried these extracts under a stream of nitrogen and then resuspended in 140 µl of mobile phase (methanol:acetonitrile 1:1). We injected 50 µl of each assay extract into an Agilent 1100 series HPLC fitted with an YMC carotenoid 5.0-µm column (4.6 mm × 250 mm, YMC) cooled to 18°C. We separated pigments with a constant mobile phase flow rate of 1.0 ml/min and a composition gradient beginning with acetonitrile:methanol (50:50) for 9 min, followed by a ramp up to acetonitrile:methanol:dichloromethane (44:44:12) (vol:vol:vol) from 9 to 11 min, isocratic through 21 min, then a second ramp up to acetonitrile:methanol:dichloromethane (35:35:30) from 21 to 26 min followed by isocratic conditions through 35 min. We monitored the sample runs with a photodiode array detector and identified putative cleavage products by comparison to authentic standards (galloxanthin, CaroteNature GmbH, Ostermundigen, Switzerland) or inferred identity from relative retention times and absorbance spectra.

Supplementary Material

Supplementary data are available at *Molecular Biology and Evolution* online.

Acknowledgments

References

Amengual J, Lobo GP, Golczak M, Li HNM, Klimova T, Hoppel CL, Wyss A, Palczewski K, von Lintig J. 2011. A mitochondrial enzyme degrades carotenoids and protects against oxidative stress. *FASEB J.* 25(3):948–959.

Andersson MB. 1994. Sexual selection. Princeton (NJ): Princeton University Press.

Andrade P, Pinho C, i de Lanuza GP, Afonso S, Brejcha J, Rubin CJ, Wallerman O, Pereira P, Sabatino SJ, Bellati A, et al. 2019. Regulatory changes in pterin and carotenoid genes underlie balanced color polymorphisms in the wall lizard. *Proc Natl Acad Sci U S A.* 116(12):5633–5642.

Birkhead TR, Schulze-Hagen K, Kinzelbach R. 2004. Domestication of the canary, *Serinus canaria*—the change from green to yellow. *Arch Nat Hist.* 31(1):50–56.

Bolger AM, Lohse M, Usadel B. 2014. Trimmomatic: a flexible trimmer for Illumina sequence data. *Bioinformatics* 30(15):2114–2120.

Chen K, Wallis JW, McLellan MD, Larson DE, Kalicki JM, Pohl CS, McGrath SD, Wendl MC, Zhang Q, Locke DP, et al. 2009. BreakDancer: an algorithm for high-resolution mapping of genomic structural variation. *Nat Methods.* 6(9):677–681.

Chothia C, Lesk AM. 1986. The relation between the divergence of sequence and structure in proteins. *EMBO J.* 5(4):823–826.

Cingolani P, Platts A, Wang LL, Coon M, Nguyen T, Wang L, Land SJ, Lu X, Ruden DM. 2012. A program for annotating and predicting the effects of single nucleotide polymorphisms, SnpEff. *Fly (Austin)* 6(2):80–92.

Clement P, Harris A, Davis J. 1993. Finches and sparrows: an identification guide. Princeton (NJ): Princeton University Press.

Dela Seña C, Sun J, Narayanasamy S, Riedl KM, Yuan Y, Curley RW, Schwartz SJ, Harrison EH. 2016. Substrate specificity of purified recombinant chicken β-carotene 9′,10′-oxygenase (BCO2). *J Biol Chem.* 291(28):14609–14619.

Emsley P, Lohkamp B, Scott WG, Cowtan K. 2010. Features and development of Coot. *Acta Crystallogr D Biol Crystallogr.* 66(4):486–501.

Eriksson J, Larson G, Gunnarsson U, Bed'hom B, Tixier-Boichard M, Strömstedt L, Wright D, Jungerius A, Vereijken A, Randi E, et al. 2008. Identification of the Yellow skin gene reveals a hybrid origin of the domestic chicken. *PLoS Genet.* 4(2):e1000010.

Fallahshahroudi A, Sorato E, Altimiras J, Jensen P. 2019. The domestic BCO2 allele buffers low-carotenoid diets in chickens-possible fitness increase through species hybridization. *Genetics* 212(4):1445–1452.

Frankl-Vilches C, Kuhl H, Werber M, Klages S, Kerick M, Bakker A, de Oliveira EHC, Reusch C, Capuano F, Vowinckel J, et al. 2015. Using the canary genome to decipher the evolution of hormone-sensitive gene regulation in seasonal singing birds. *Genome Biol.* 16(1):25.

Garrison E, Marth G. 2012. Haplotype-based variant detection from short-read sequencing. arXiv Prepr. arXiv1207.3907:9.

Goldsmith TH, Collins JS, Licht S. 1984. The cone oil droplets of avian retinas. *Vision Res.* 24(11):1661–1671.

Hall TA. 1999. BioEdit: a user-friendly biological sequence alignment editor and analysis program for Windows 95/98/NT. *Nucleic Acids Symp Ser.* 41:95–98.

Hill GE, McGraw KJ. 2006a. Bird coloration: mechanisms and measurements. Vol. 1. Boston (MA): Harvard University Press.

Hill GE, McGraw KJ. 2006b. Bird coloration: function and evolution. Vol. 2. Boston (MA): Harvard University Press.

Hubbard JK, Uy JAC, Hauber ME, Hoekstra HE, Safran RJ. 2010. Vertebrate pigmentation: from underlying genes to adaptive function. *Trends Genet.* 26(5):231–239.

Huggins KA, Navara KJ, Mendonça MT, Hill GE. 2010. Detrimental effects of carotenoid pigments: the dark side of bright coloration. *Naturwissenschaften* 97(7):637–644.

Iverson ENK, Karubian J. 2017. The role of bare parts in avian signaling. *Auk* 134(3):587–611.

Kiefer C, Hessel S, Lampert JM, Vogt K, Lederer MO, Breithaupt DE, Von Lintig J. 2001. Identification and characterization of a mammalian enzyme catalyzing the asymmetric oxidative cleavage of provitamin A. *J Biol Chem.* 276(17):14110–14116.

Kiser PD, Golczak M, Lodowski DT, Chance MR, Palczewski K. 2009. Crystal structure of native RPE65, the retinoid isomerase of the visual cycle. *Proc Natl Acad Sci U S A.* 106(41):17325–17330.

Kloer DP, Ruch S, Al-Babili S, Beyer P, Schulz GE. 2005. The structure of a retinal-forming carotenoid oxygenase. *Science* 308(5719):267–269.

Koch RE, McGraw KJ, Hill GE. 2016. Effects of diet on plumage coloration and carotenoid deposition in red and yellow domestic canaries (*Serinus canaria*). *Wilson J Ornithol.* 128(2):328–333.

Kofler R, Pandey RV, Schlötterer C. 2011. PoPoolation2: identifying differentiation between populations using sequencing of pooled DNA samples (Pool-Seq). *Bioinformatics* 27(24):3435–3436.

Layer RM, Chiang C, Quinlan AR, Hall IM. 2014. LUMPY: a probabilistic framework for structural variant discovery. *Genome Biol.* 15(6):R84.

Li H, Durbin R. 2010. Fast and accurate long-read alignment with Burrows–Wheeler transform. *Bioinformatics* 26(5):589–595.

Lobo GP, Amengual J, Palczewski G, Babino D, von Lintig J. 2012. Mammalian carotenoid-oxygenases: key players for carotenoid function and homeostasis. *Biochim Biophys Acta Mol Cell Biol Lipids* 1821(1):78–87.

Lobo GP, Isken A, Hoff S, Babino D, von Lintig J. 2012. BCDO2 acts as a carotenoid scavenger and gatekeeper for the mitochondrial apoptotic pathway. *Development* 139(16):2966–2977.

Lopes RJ, Johnson JD, Toomey MB, Ferreira MS, Araujo PM, Melo-Ferreira J, Andersson L, Hill GE, Corbo JC, Carneiro M. 2016. Genetic basis for red coloration in birds. *Curr Biol.* 26(11):1427–1434.

Mayr E. 1963. Animal species and evolution. Cambridge (MA): Harvard University Press.

McGraw KJ, Hudon J, Hill GE, Parker RS. 2005. A simple and inexpensive chemical test for behavioral ecologists to determine the presence of carotenoid pigments in animal tissues. *Behav Ecol Sociobiol.* 57(4):391–397.

McKenna A, Hanna M, Banks E, Sivachenko A, Cibulskis K, Kernytsky A, Garimella K, Altshuler D, Gabriel S, Daly M, et al. 2010. The Genome Analysis Toolkit: a MapReduce framework for analyzing next-generation DNA sequencing data. *Genome Res.* 20(9):1297–1303.

Mein JR, Dolnikowski GG, Ernst H, Russell RM, Wang XD. 2011. Enzymatic formation of apo-carotenoids from the xanthophyll carotenoids lutein, zeaxanthin and β-cryptoxanthin by ferret carotene-9′,10′-monooxygenase. *Arch Biochem Biophys.* 506(1):109–121.

Mundy NI, Stapley J, Bennison C, Tucker R, Twyman H, Kim K-W, Burke T, Birkhead TR, Andersson S, Slate J. 2016. Red carotenoid coloration in the zebra finch is controlled by a cytochrome P450 gene cluster. *Curr Biol.* 26(11):1435–1440.

Rausch T, Zichner T, Schlattl A, Stütz AM, Benes V, Korbel JO. 2012. DELLY: structural variant discovery by integrated paired-end and split-read analysis. *Bioinformatics* 28(18):i333–i339.

Robinson JT, Thorvaldsdóttir H, Winckler W, Guttman M, Lander ES, Getz G, Mesirov JP. 2011. Integrative genomics viewer. *Nat Biotechnol.* 29(1):24–26.

Singh J, Thornton JM, Snarey M, Campbell SF. 1987. The geometries of interacting arginine-carboxyls in proteins. *FEBS Lett.* 224(1):161–171.

Strychalski J, Brym P, Czarnik U, Gugołek A. 2015. A novel AAT-deletion mutation in the coding sequence of the BCO2 gene in yellow-fat rabbits. *J Appl Genet.* 56(4):535–537.

Tian R, Pitchford WS, Morris CA, Cullen NG, Bottema C. 2010. Genetic variation in the β,β-carotene-9′,10′-dioxygenase gene and association with fat colour in bovine adipose tissue and milk. *Anim Genet.* 41(3):253–259.

Toews DPL, Hofmeister NR, Taylor SA. 2017. The evolution and genetics of carotenoid processing in animals. *Trends Genet.* 33(3):171–182.

Toews DPL, Taylor SA, Vallender R, Brelsford A, Butcher BG, Messer PW, Lovette IJ. 2016. Plumage genes and little else distinguish the genomes of hybridizing warblers. *Curr Biol.* 26(17):2313–2318.

Toomey MB, Collins AM, Frederiksen R, Cornwall MC, Timlin JA, Corbo JC. 2015. A complex carotenoid palette tunes avian colour vision. *J R Soc Interface* 12(111):20150563.

Toomey MB, Corbo JC. 2017. Evolution, development and function of vertebrate cone oil droplets. *Front Neural Circuits* 11:97.

Toomey MB, Lind O, Frederiksen R, Curley RW, Riedl KM, Wilby D, Schwartz SJ, Witt CC, Harrison EH, Roberts NW, et al. 2016. Complementary shifts in photoreceptor spectral tuning unlock the full adaptive potential of ultraviolet vision in birds. *Elife* 5:e15675.

Toomey MB, Lopes RJ, Araújo PM, Johnson JD, Gazda MA, Afonso S, Mota PG, Koch RE, Hill GE, Corbo JC, et al. 2017. High-density lipoprotein receptor SCARB1 is required for carotenoid coloration in birds. *Proc Natl Acad Sci U S A.* 114(20):5219–5224.

Våge DI, Boman IA. 2010. A nonsense mutation in the beta-carotene oxygenase 2 (BCO2) gene is tightly associated with accumulation of carotenoids in adipose tissue in sheep (*Ovis aries*). *BMC Genet.* 11(1):10.

Walker GBR, Avon D. 1993. Coloured, type, and song canaries: a complete guide. London, United Kingdom: Blandford Press.

Waterhouse A, Bertoni M, Bienert S, Studer G, Tauriello G, Gumienny R, Heer FT, de Beer TAP, Rempfer C, Bordoli L, et al. 2018. SWISS-MODEL: homology modelling of protein structures and complexes. *Nucleic Acids Res.* 46(W1):W296–W303.

Yanishlieva NV, Aitzetmüller K, Raneva V. 1998. β-Carotene and lipid oxidation. *Lipid Fett* 100(10):444–462.

Zhang J, Kiser PD, Badiee M, Palczewska G, Dong Z, Golczak M, Tochtrop GP, Palczewski K. 2015. Molecular pharmacodynamics of emixustat in protection against retinal degeneration. *J Clin Invest.* 125(7):2781–2794.